Supporting Information

The MOF-derived CoFe Alloy Nanoparticles Encapsulated Within N, O Co-doping Multilayer Graphitized Shells as Efficient Bifunctional Catalyst for Zinc-air Battery

*Jingjing Zhang, Fumin Tang, Kechuang Wan, Yange Yang, Cunman Zhang, Pingwen Ming, Bing Li**

Dr. J.J. Zhang, *F.M. Tang, K.C. Wan, Y.G. Yang, C. Feng,* Prof. *C.M. Zhang, P.W. Ming, B. Li*

Clean Energy Automotive Engineering Center and School of Automotive Studies, Tongji University, Shanghai 201804, China;
Email: libing210@tongji.edu.cn

Experimental Section

1.1. Synthesis of CoFe@NOC

The CoFe@NOC was synthesized as follows: First, 0.466 mmol 3.3'-Diaminobenzidine (DAB), 0.369mmol $FeCl_3 \cdot 6H_2O$, (0.6mmol / 1.2mmol / 2.4mmol) Co $(NO_3)_2 \cdot 6H_2O$, 0.55mmol 2-Aminoterephthalic acid (HPLC) were added with 30 mL of DMF and that was ultrasound for 10 min, with continuous stirring for half an hour. Second, the mixture was played in a Teflon-lined autoclave (50 mL) for 12 hours at 100℃, 120℃, 140℃, respectively. The orange products were washed with DMF and ethanol and recovered by centrifugation. Third, the pyrolyzed composites were thermally treated at 650℃, 750℃, 850℃ for 3 hours under nitrogen atmosphere. The CoFe@NOC electrocatalysts was eventually achieved. For comparison, the Co@NOC was synthetized without the $FeCl_3 \cdot 6H_2O$. The Fe@NOC was synthetized without the Co $(NO_3)_2 \cdot 6H_2O$.

Synthesis of Co@NOC: Co@NOC was prepared in the same way as CoFe@NOC, except no $FeCl_3 \cdot 6H_2O$ was added to the solution.

Synthesis of Fe@NOC: Fe@NOC was prepared in the same way as CoFe@NOC, except no Co $(NO_3)_2 \cdot 6H_2O$ was added to the solution.

1.2. Characterization

The as-obtained products were characterized with X-ray diffraction (XRD) (Bruker D8) using Cu Kα radiation (λ = 0.15406 nm), SEM, and energy-dispersive X-ray analysis (Nova Nano SEM 200) operated at an acceleration voltage of 10 kV, and TEM and HRTEM (JEM-2100, JEOL). Energy-dispersive X-ray spectroscopy was

taken at the same time as TEM measurement. Raman spectroscopy (JY-T 643200, France) was performed at ambient temperature with a laser excitation of 514 nm. XPS was performed on a spectrometer from Kratos Axis Ultradld, using Mono Al Kα radiation at a power of 120 W (8 mA, 15 kV). The nitrogen adsorption/desorption data were recorded at the liquid nitrogen temperature (77 K) using a micrometrics apparatus (ASAP 2020 M). The specific surface area was calculated using the BET equation. Microstructure of CoFe@NOC powder was captured using a microscope (Olympus BX51). The density was measured with a TD-1200 True Density Tester.

XAFS measurements. The XAFS data were collected at BL14W1 station in SSRF (Shanghai Synchrotron Radiation Facility). The acquired XAFS data were processed according to the standard procedures using the ATHENA module implemented in the IFEFFIT software packages. The k^3-weighted EXAFS spectra were obtained by subtracting the post-edge background from the overall absorption and then normalizing with respect to the edge-jump step.

1.3. Electrochemical measurements

Prior to the surface coating, glassy carbon rotating disk electrode (RDE, 5 mm in diameter) was polished carefully with 1.0, 0.3 and 0.05μm alumina powder, respectively, and rinsed with deionized water, followed by sonicated in ethanol and doubly distilled water successively. All catalysts were prepared by mixing 2 mg of the catalysts in 1 mL of solution containing 480 μL of ethanol, 480 μL of H_2O and 4 μL of 5% Nafion solution, followed by ultrasonication for 30 min to form homogeneous catalysts inks. The obtained catalysts inks were then dropped on the surface of

pretreated RDE surface and dried before the electrocatalytic tests, leading to 0.2 and 0.1 mg cm^{-2} loading for the obtained samples and Pt/C, respectively.

All the electrochemical measurements were carried out on WaveDriver 20 (Pine Research Instrumentation) and CHI 660E Potentiostat (CH Instruments) systems equipped with a three-electrode cell. All the measurements were performed at ambient temperature in a 0.1 M KOH alkaline solution. A glassy carbon electrode (GCE) coated with the catalyst ink was served as the working electrode, a Hg/HgO and Carbon rod wire were used as reference and counter electrode, respectively. Potentials in this work were all referred to the reversible hydrogen electrode (RHE) through the Nernst equation as follows: E (vs. RHE) =E (vs. Hg/HgO) + 0.098 +0.0591 × pH. Prior to the measurement, a N_2/O_2 flow was used through the electrolyte in the cell for 30 min to saturate it with N_2/O_2. The electrochemical experiments were conducted in O_2-saturated 0.1 M KOH for the oxygen reduction reaction at room temperature. The RDE tests were measured at various rotating speed from 400 to 2500 rpm with a sweep rate of 5 mV s^{-1}. For the ORR at an RDE, the electron transfer number (n) and kinetic current density (J_K) were calculated from the Koutecky-Levich (K-L) equation:

$$\frac{1}{J} = \frac{1}{J_L} + \frac{1}{J_K} = \frac{1}{B\omega^{\frac{1}{2}}} + \frac{1}{J_K}$$

$$B = 0.62nFC_0D_0^{\frac{2}{3}}V^{\frac{1}{6}}$$

where J is the measured current density, J_K and J_L are the kinetic and limiting current densities, ω is the angular velocity of the disk, n is the electron transfer number, F is the Faraday constant (96485 C mol^{-1}), C_0 is the bulk concentration of O_2 (1.2×10^{-6}

mol cm^{-3}), D_0 is the diffusion coefficient of O_2 (1.9×10^{-5} cm^2 s^{-1}), and V is the kinematic viscosity of the electrolyte (0.01 cm^2s^{-1}).

The accelerated durability tests (ADT) of the electrocatalysts were performed in the O_2-saturated 0.1 M KOH electrolyte at room temperature by chronoamperometric responses at a constant potential of 0.7 V for 108000 s.

1.4. Electrochemical measurements for Zn-air battery

The primary Zn-air batteries were tested in a home-built electrochemical cell. The homogeneous ink was loaded on carbon fiber paper (1 cm^2), with a loading density of 1 mg cm^{-2}. as the air cathode, and a polished Zn foil was used as the anode. A 0.2 M Zn $(OAc)_2$ in 6M KOH aqueous solution was used as the electrolyte. All data were collected from the as-fabricated cell with a Land CT2001A system at room temperature.

2.5. DFT Computational

All the theoretical computations were performed by the Vienna ab initio simulation package (VASP). The generalized gradient approximation (GGA) with a Perdew–Burke–Ernzerhof (PBE) functional was used to describe the electronic exchange and correlation effects, and the plane-wave cutoff was tested and set to 400 eV. The selfconsistent field (SCF) tolerance was 1×10^{-4} eV. The Brillouin zone was sampled at a ($2 \times 2 \times 1$) mesh. The surface models were built based on the TEM and XRD results of the CoFe@NOC, Co@NOC, and Fe@NOC catalysts。

The Gibbs free energy (G) was calculated as $G = E_{surf} + E_{ZPE} - T\Delta S$, where E_{surf} is the total energy calculated via DFT, and EZPE is the zero-point energy calculated using the vibrational frequencies of the adsorbates.

The oxygen evolution reaction (OER) mechanism was proposed to involve four steps with the intermediates of OH*, O*, and OOH*. This method was developed by Nørskov et. al. Here, the * represents the reaction active sites located at the surface of structure model. Usually, the oxygen atom of reaction intermediates was connected to the active sites, forming a single bond. The largest absorption free energy variation of each step was defined as theoretical values of over-potential (η), which determines the rate of overall reaction. The computational hydrogen electrode was used to obtain free energies for each state as done in previous paper. The four electron OER pathway could be summarized by the following four elementary steps:

$$* + H_2O \rightarrow OH* + H^* + e^- \qquad \Delta G_1$$

$$OH* \rightarrow O* + H^+ e^- \qquad \Delta G_2$$

$$O* + H_2O \rightarrow OOH* + H^+ + e^- \qquad \Delta G_3$$

$$OOH* \rightarrow * + O_2 + H^+ + e^- \qquad \Delta G_4$$

Chemicals:

N, N-Dimethylformamide (DMF) were obtationed from Sigma-Aldrich. 2-Aminoterephthalic Acid (HPLC), 3.3'-Diaminobenzidine (DAB) were purchased from aladdin. Ethanol absolute, $FeCl_3 \cdot 6H_2O$, Co $(NO_3)_2 \cdot 6H_2O$, KOH was purchased from Sinopharm Chemical Reagent Co., Ltd. Nafion perfluorinated resin solution (5 wt. % in mixture of lower aliphatic a lcohols and water, contains 45% water), All the

reagents were of analytical grade and used as received without further purification. Deionized water was used throughout the experimental processes.

Results and Discussion

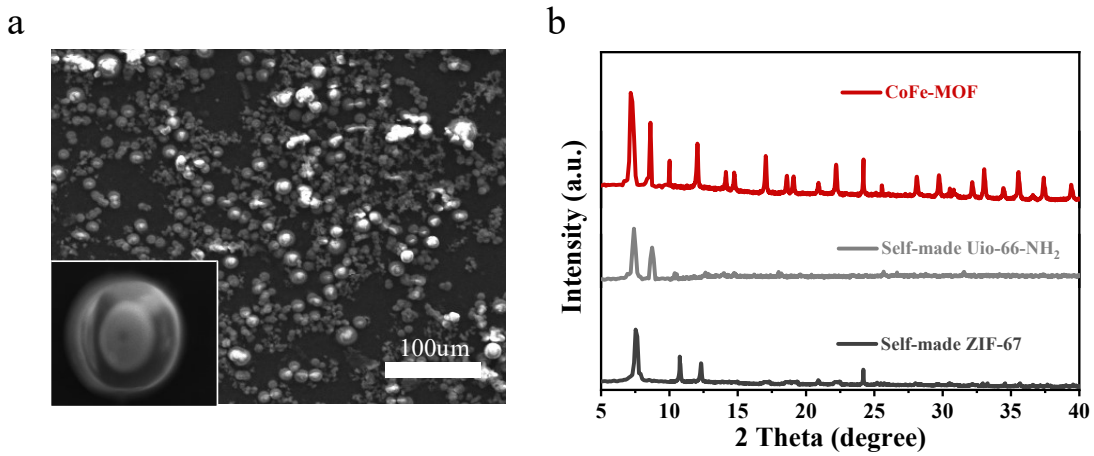

Fig. S1. a) SEM images of hybrid CoFe-MOF precursors; b) XRD patterns of hybrid CoFe-MOF precursors.

The morphologies of the catalysts before pyrolysis were studied by scanning electron microscopy (SEM). As shown in Fig. S1a, the CoFe-MOF precursors show the regular crystal ball-like and irregular granular. Crystal ball-like hybrid CoFe-MOF consists of ZIF-67 and Uio-66-NH_2, which is confirmed by XRD (Fig. S1b), [1,2] has been fabricated as an advanced precursor.

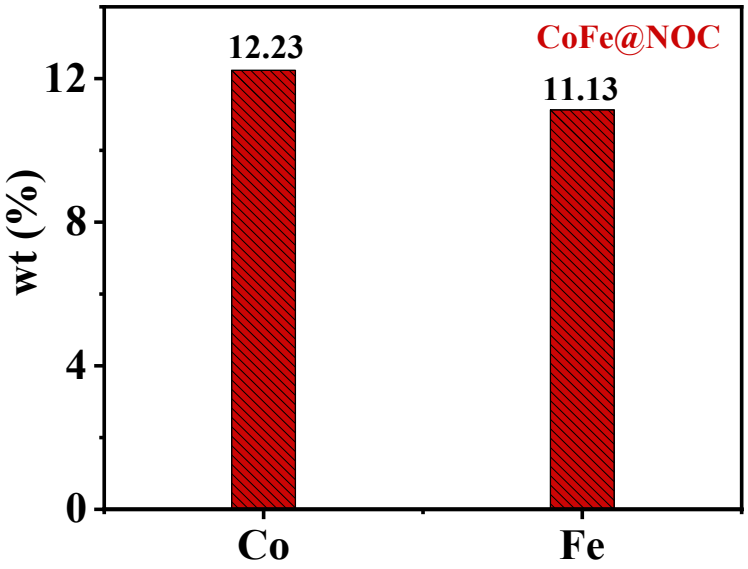

Fig. S2. Chart showing the percentage of cobalt and iron in the materials (CoFe@NOC) measured by ICP-MS.

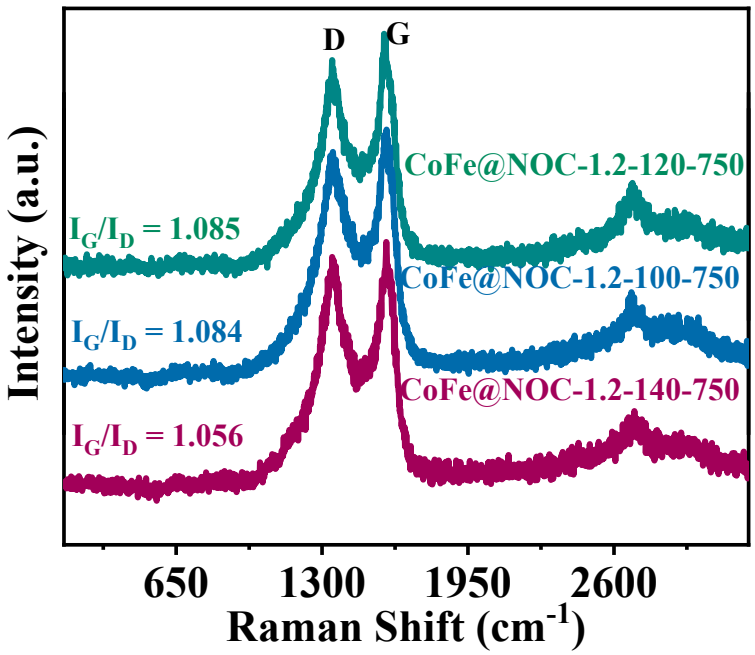

Fig. S3. Raman spectra of CoFe@NOC-1.2-120-750, CoFe@NOC-1.2-100-750 and CoFe@NOC-1.2-140-750.

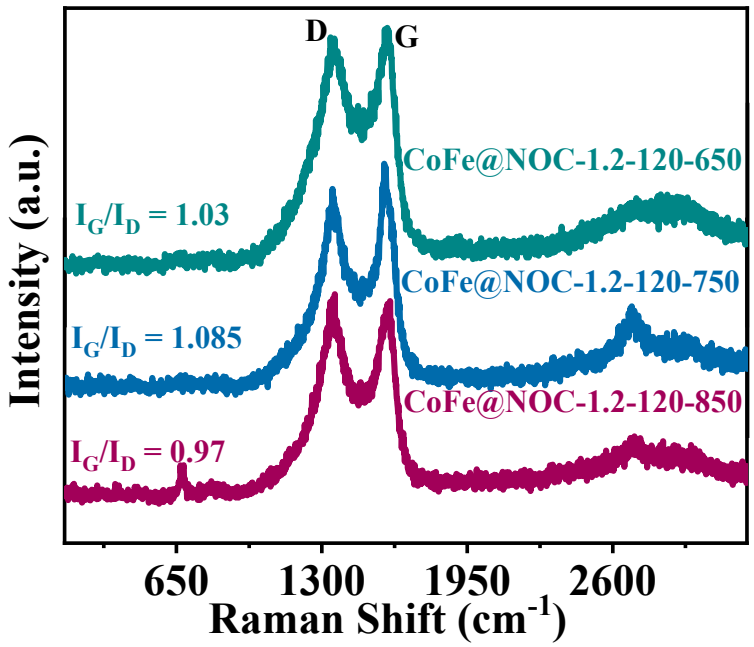

Fig. S4. Raman spectra of CoFe@NOC-1.2-120-650, CoFe@NOC-1.2-120-750 and CoFe@NOC-1.2-120-850.

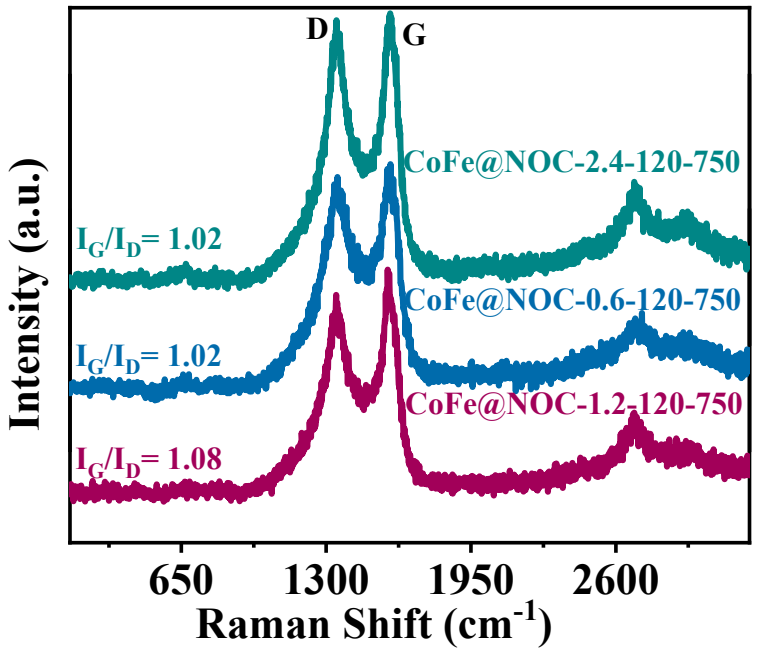

Fig. S5. Raman spectra of CoFe@NOC-0.6-120-750, CoFe@NOC-1.2-120-750 and CoFe@NOC-2.4-120-750.

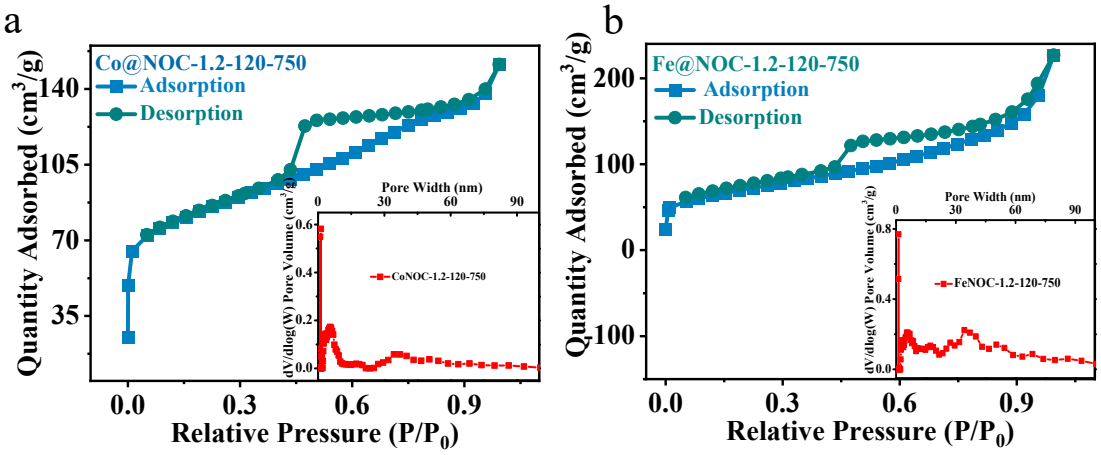

Fig. S6. The nitrogen adsorption–desorption isotherms, and the corresponding pore size distribution. a) Co@NOC-1.2-120-750; b) Fe@NOC-1.2-120-750.

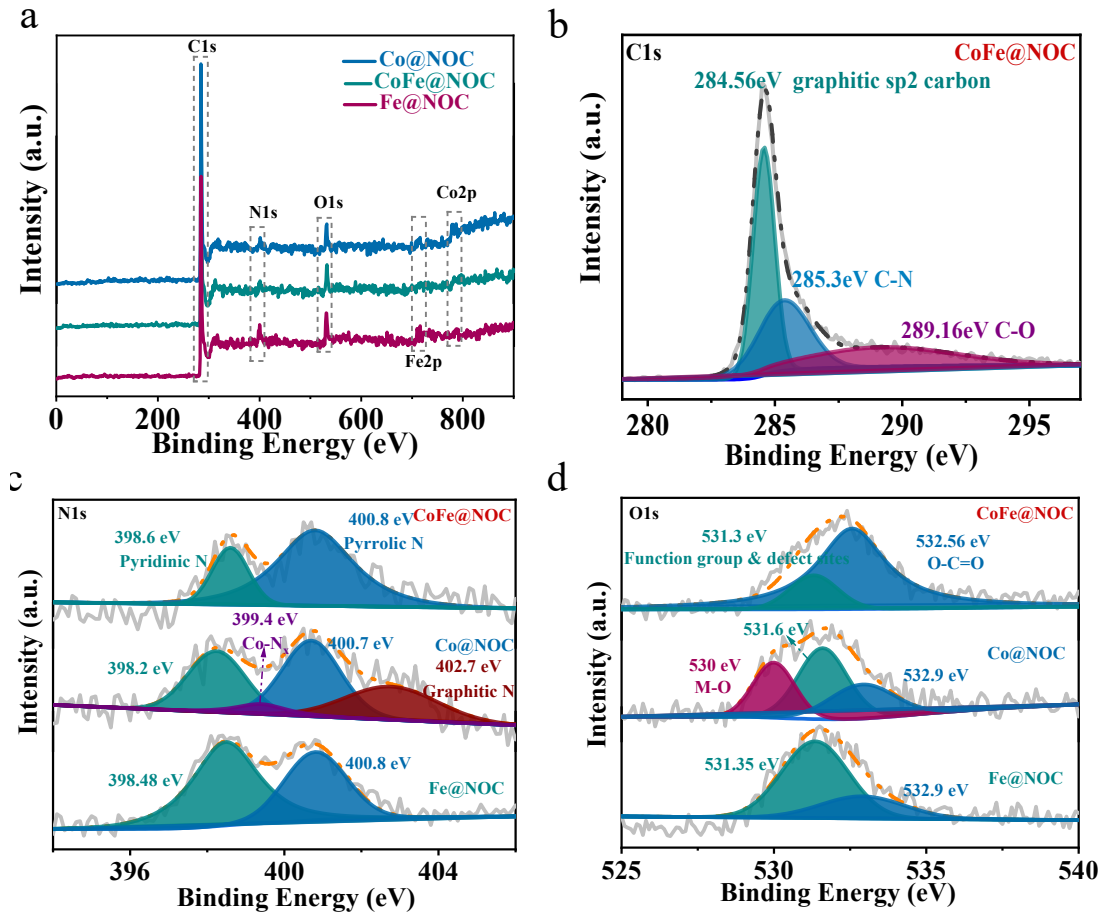

Fig. S7. XPS spectra of: a) CoFe@NOC, Co@NOC and Fe@NOC; b) C1s for CoFe@NOC; c) N 1s for CoFe@NOC, Co@NOC, and Fe@NOC; d) O 1s for CoFe@NOC, Co@NOC, and Fe@NOC.

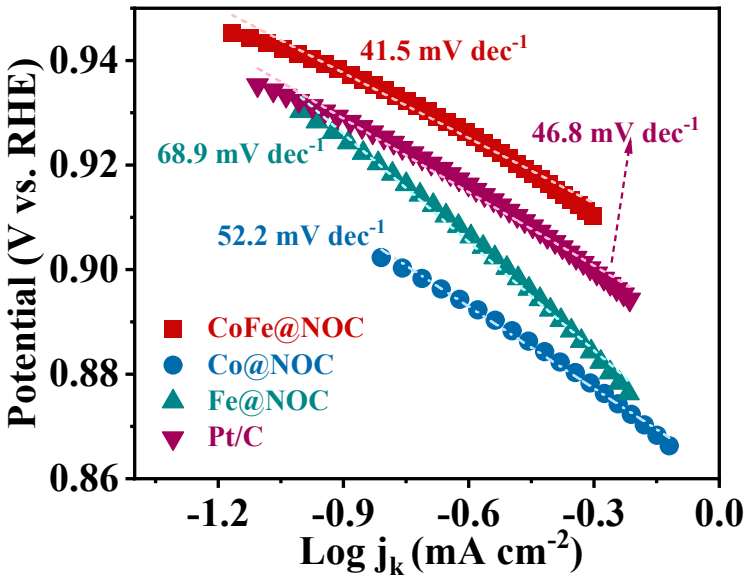

Fig. S8. The corresponding Tafel plots for the ORR.

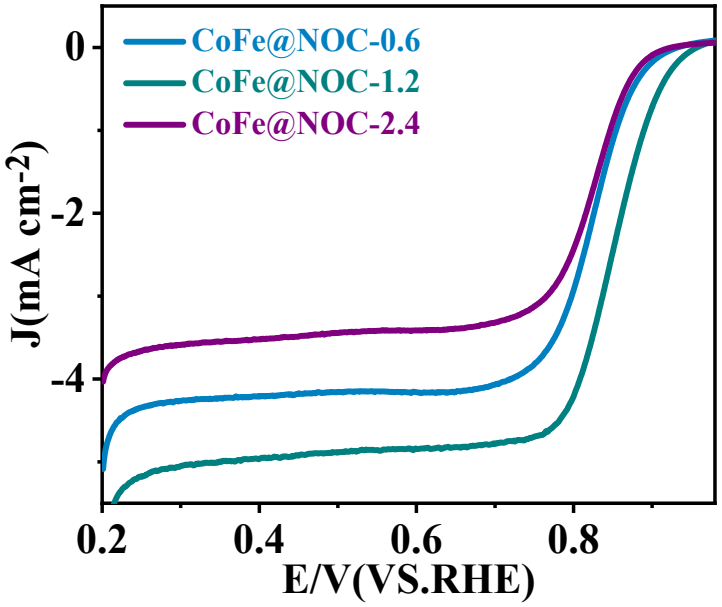

Fig. S9. ORR performance: LSV curves of CoFe@NOC-0.6-120-750, CoFe@NOC-1.2-120-750 and CoFe@NOC-2.4-120-750 at 1600 rpm.

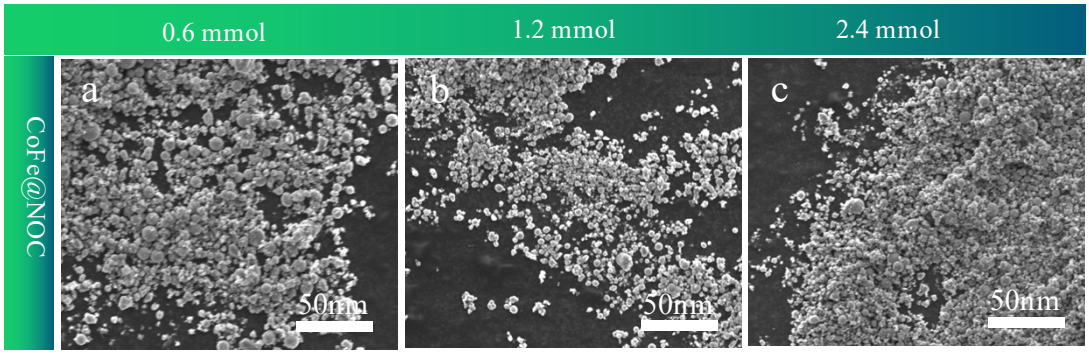

Fig. S10. SEM images of CoFe@NOC (different molar ratio of Co $(NO_3)_2 \cdot 6H_2O$).

we did a series of contrast experiment under the same conditions to identify the role of different molar ratio of Co $(NO_3)_2 \cdot 6H_2O$. As can be seen from Fig.S10, we found that the morphologies were very similar, indicating that different molar ratio of Co $(NO_3)_2 \cdot 6H_2O$ had little effect on the sample morphologies.

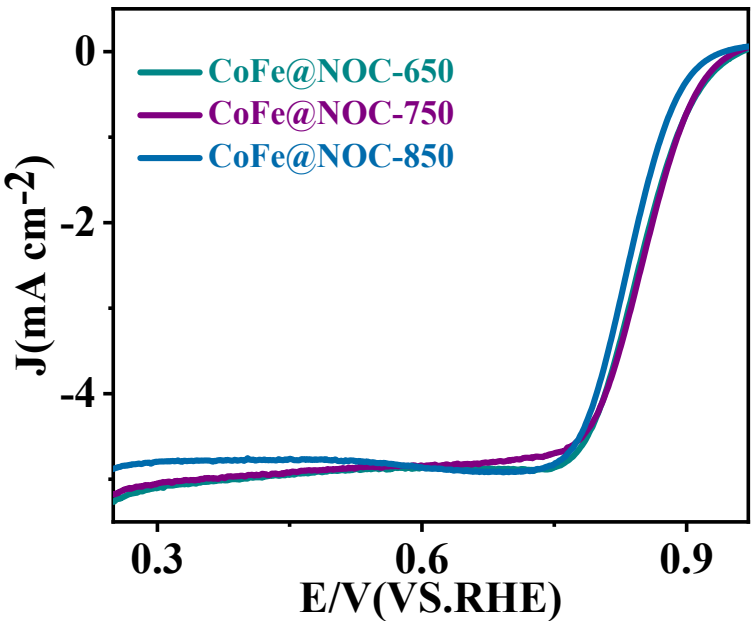

Fig. S11. ORR performance: LSV curves of CoFe@NOC-1.2-120-650, CoFe@NOC-1.2-120-750 and CoFe@NOC-1.2-120-850 at 1600 rpm.

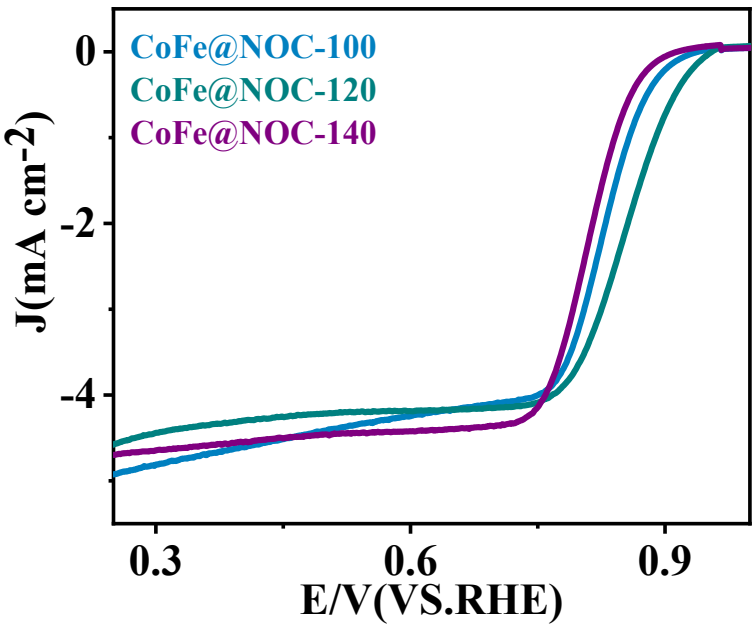

Fig. S12. ORR performance: LSV curves of CoFe@NOC-1.2-100-750, CoFe@NOC-1.2-120-750, CoFe@NOC-1.2-140-750 and 20wt% Pt/C at 1600 rpm.

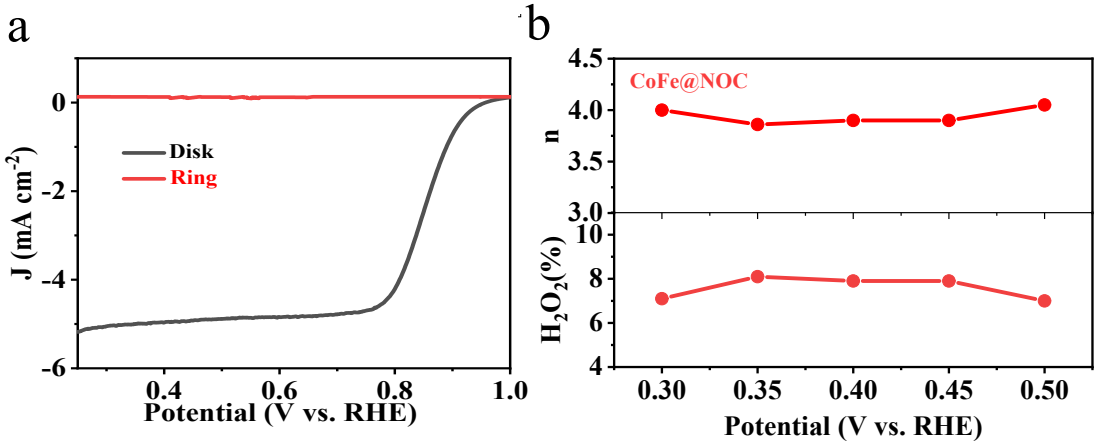

Fig. S13. the test was performed at 1600 rpm in O_2-saturated 0.1 M KOH electrolyte. a) Rotating ring-disk electrode voltammograms of CoFe@NOC; b) Corresponding electron transfer numbers and H_2O_2 yields in the potential range 0.3 ~ 0.5 V.

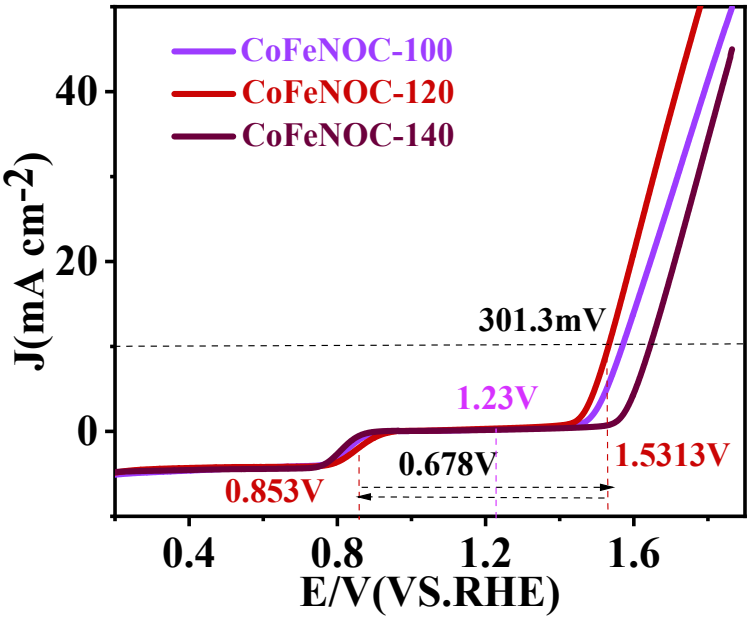

Fig. S14. Comparison of ORR and OER performance in O_2-saturated 0.1 M KOH for CoFe@NOC-100, CoFe@NOC-120, and CoFe@NOC-140: the overall polarization curves within the ORR and OER potential window.

The CoFe@NOC was also superior in e electrocatalytically active surface area (ECSA), as investigated via double-layer capacitance (Cdl) and CV measurements (Fig. S15). The highest value of CoFe@NOC (54.7 mF cm^{-2}) indicates that more active sites can be exposed in CoFe@NOC, in line with the more excellent OER performance. [5,6]

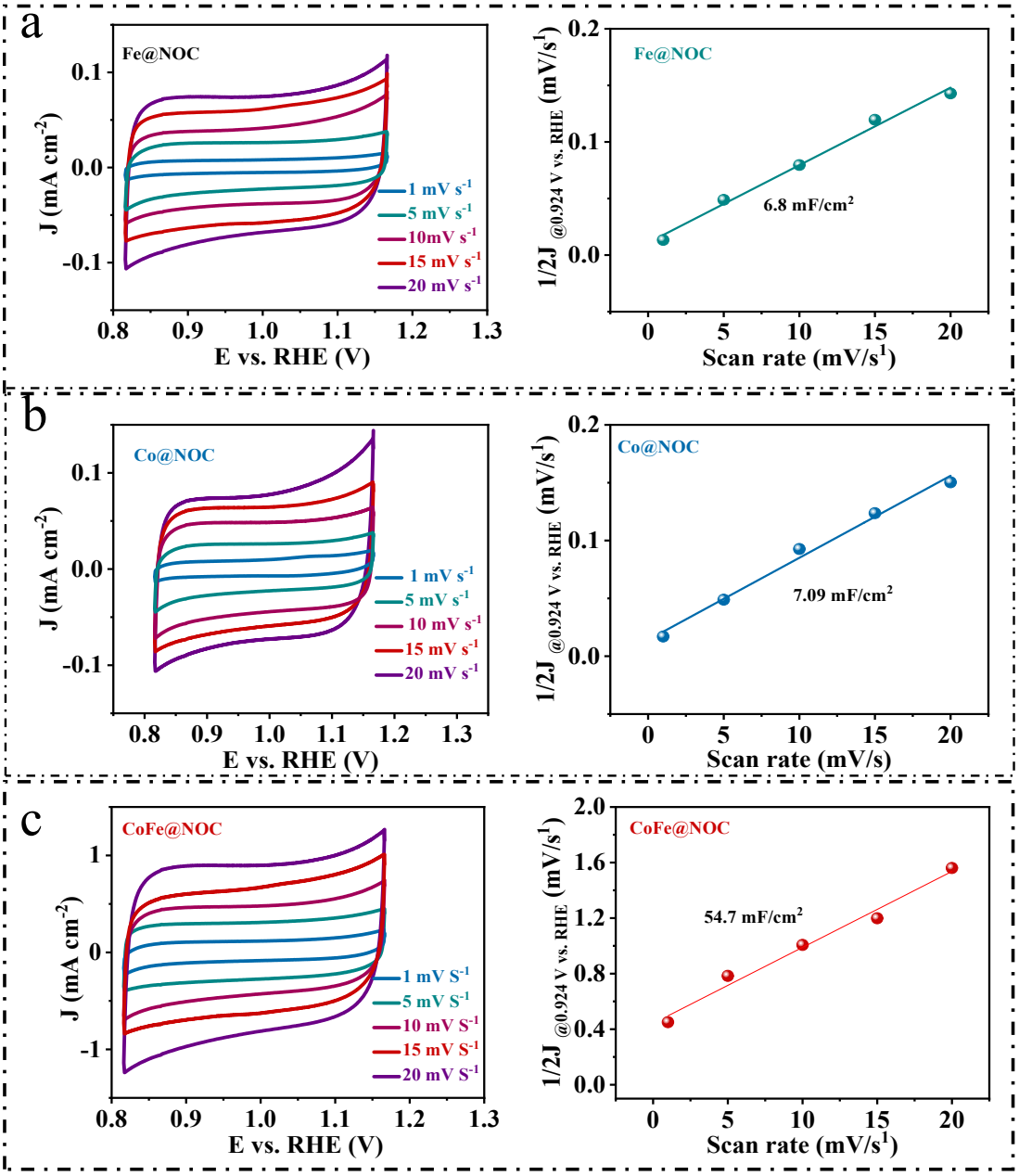

Fig. S15. Comparison of CV curves and half of the capacitive current density difference at 0.92 V as a function in 0.1 m KOH: a) Fe@NOC; b) Co@NOC; c) CoFe@NOC.

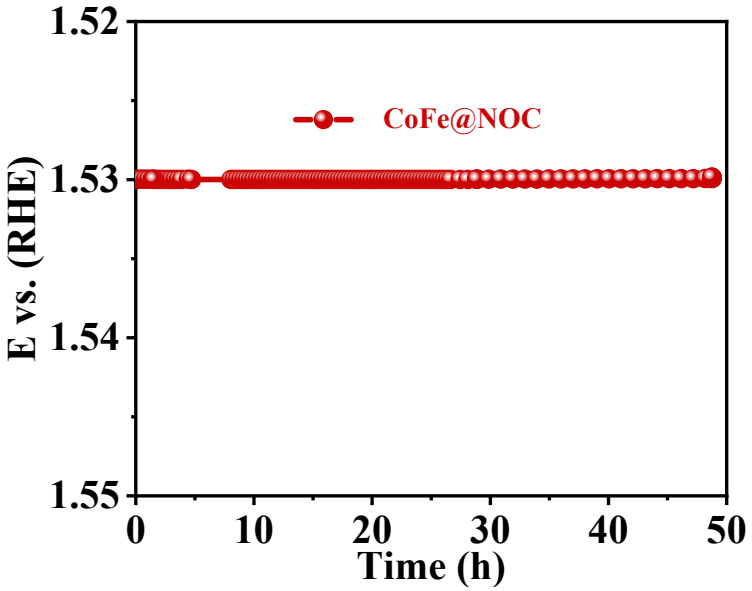

Fig. S16. chronopotentiometry curves at a constant current density of 10 mA cm^{-2}.

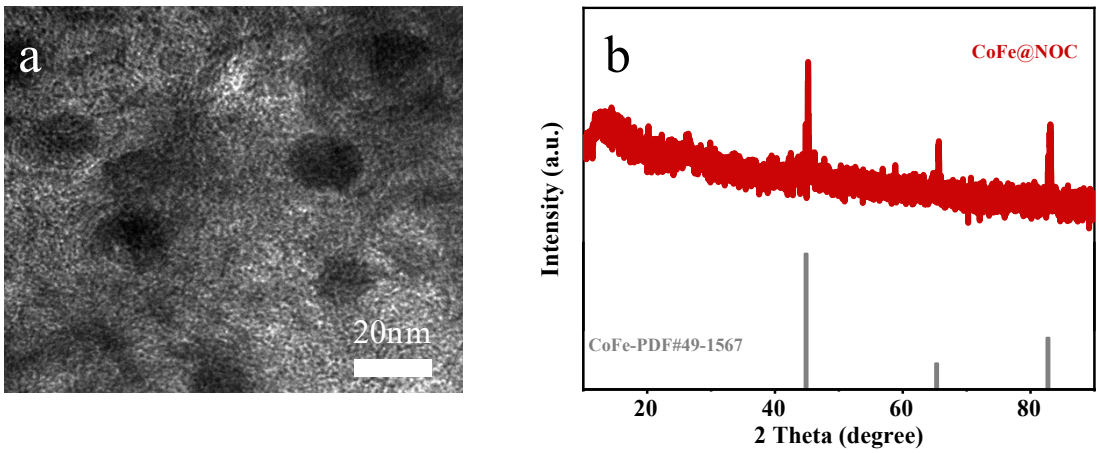

Fig. S17. a) TEM image; b) XRD pattern of CoFe@NOC after the long-term charge/discharge cycles.

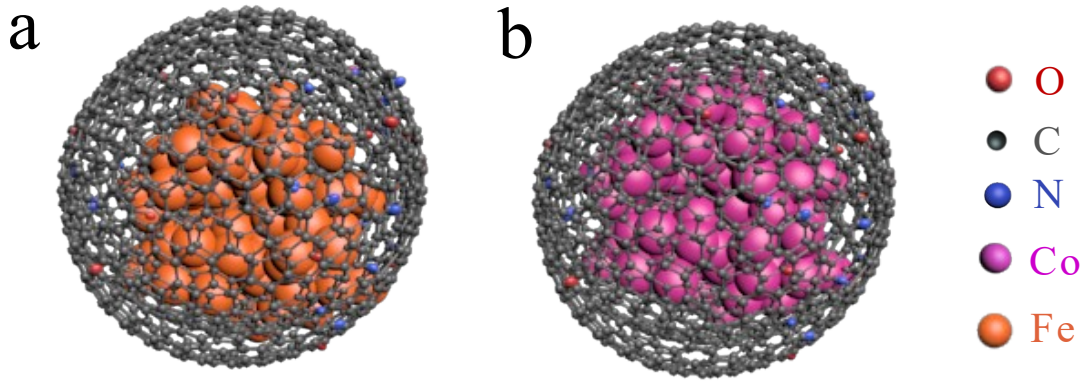

Fig. S18. Schematic mechanism of the whole OER cycle on the a） Fe@NOC and b) Co@NOC in the alkaline electrolyte

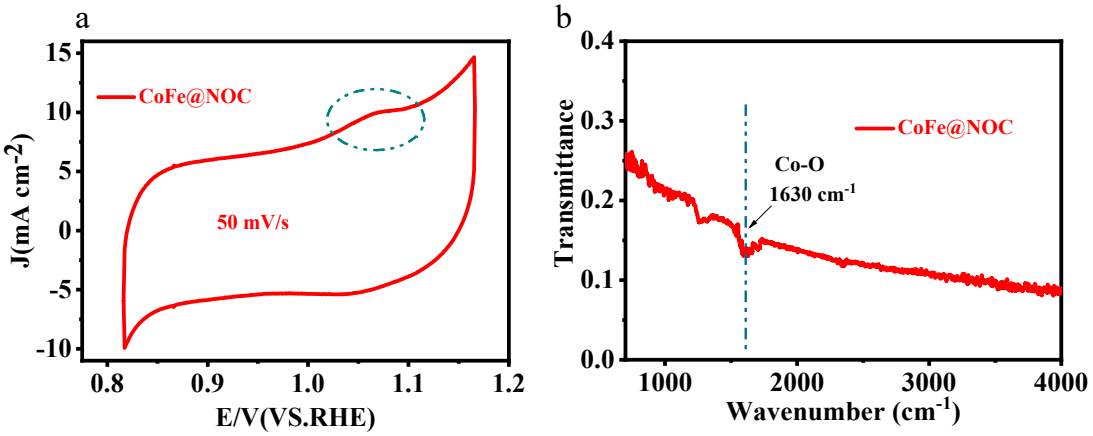

Fig. S19. a) CV curves of CoFe@NOC at 10 mV s^{-1}; b) The FTIR spectra of FeCo@NOC samples after zinc-air battery test in 0.1 M KOH.

Table S1. Summary of reported ORR performance of metal-doped carbon catalysts. All catalysts were evaluated in an O_2-saturated 0.1 M KOH aqueous solution

Catalysts	**Onset potential (V vs. RHE)**	**$E_{1/2}$ (V vs. RHE)**	**Durability (h)**	**Reference**
MnO/Co/PGC	0.95	0.78	5.5	Adv. Mater. 2019, 31, 1902339.
Co@N-PCP/NB-CNF-2-800	1.01	0.85	10000 cycles	Appl. Catal. B-Environ. 2021, 286, 119858.
1@ZnCo-ZIF	0.85	0.8	6	Angew. Chem. Int. Ed. 2021, 60, 8472-8476.
Co_9−xNixS_8/NC	0.912	0.864	5.5	ACS Appl. Mater. Interfaces 2020, 12, 5847-5856.
$CuMo_2ON$@NG	0.956	0.875	11	Nano Energy 2021, 85, 105987.
CoFe@NC/KB-800	0.95	0.845	14	Chem. Eng. J. 2022, 427, 131614.
Co, Nb-MoS_2/TiO_2 HSs	0.96	0.86	17	Nano Energy 2021, 82, 105750.
$CuCoF_2$@PCNFs	1	0.84	1000 cycles	Nano Lett 2021, 21, 2618-2624.
FeCoNiOx@IrPt	0.93	0.83		Adv. Energy Mater. 2020, 10, 2001119.
$NiCo_2O_4$-450-Vo		0.75	5.5	Appl. Catal. B-Environ. 2021, 291, 120065.
Co/Co_3O_4@PGS	0.97	0.89	8.3	Ad. Energy Mater. 2018, 8, 1702900.
co-doped np-graphene	0.987	0.845	50	Add. Mater. 2019, 31, 1900843.
Cu-N-C	~0.96	0.869	~3	Energy Environ. Sci. 2018, 11, 2263.
Co-ISAS/p-CN	~0.90	0.838	5000 cycles	Adv. Mater. 2018, 30, 1706508.
Fe-NC SAC	0.98	0.9		Nat. Commun. 2019, 10, 1278.
Cu-SAs/N-C	0.99	0.895	5000 cycles	Nat. Catal. 2018, 1, 781.
Fe_2-Z_8-C	0.985	0.871	~3	Angew. Chem., Int. Ed. 2018, 57, 1204.
Fe-N-C-900	0.99	0.927	~14	Adv. Energy Mater.2018, 8, 1801956.
Fe-N-SCCFs	1.03	0.883		Nano Lett. 2017, 17, 2003.
CoZIF-VXC72	~0.94	0.84	10000 cycles	Adv. Mater. 2017, 29, 1701354.
NC@Co-NGC DSNCs	0.92	0.82		Adv. Mater. 2017, 29, 1700874.
h-Mn_3O_4-MSLs	0.91	0.84		J. Am. Chem. Soc. 2017, 139, 12133.
CoOx NPs/BNG	0.95	0.81	6000 cycles	Angew. Chem., Int. Ed. 2017, 56, 7121.
20wt% Pt/C	0.91	0.83	30	This work
CoFe@NOC	0.96	0.85	30	This work

Table S2. Comparison of the electrocatalytic activities of CoFe@NOC some representative bifunctional electrocatalysts reported in 0.1 M KOH solution. catalysts were evaluated in an

Catalysts	E_{j10} (V)	$E_{1/2}$ (V)	$\Delta E = (E_{j10}-E_{1/2})$ (V)	Reference
MnO/Co/PGC	1.6	0.78	0.82	Adv. Mater. 2019, 31, 1902339.
Ni-MnO/rGO aerogel	1.6	0.78	0.82	Adv. Mater. 2018, 30, 1704609
ZnCo@NC	1.71	0.80 V	0.91	Angew. Chem. Int. Ed. 2021, 15, 8472-8476
Fe_3C-Co/NC	1.57	~	~	Adv. Funct. Mater. 2019, 29, 1901949
PHI-Co	1.554	~	~	Adv. Mater. 2020, 32, 1903942
Fe-Co_3O_4	1.492	~	~	Adv. Mater. 2020, 32, 2002235
NiO/Co_3O_4	1.492	~	~	ACS Catal. 2020, 10, 12376
$Ba_4Sr_4(Co_{0.8}Fe_{0.2})_4O_{15}$	1.57	~	~	Adv. Mater. 2020, 32, 1905025.
$LaCo_1$-x$NixO_3$-δ	1.56	~	~	Angew. Chem., Int. Ed. 2020, 59, 19691
Co9−x$NixS_8$/NC	1.652	0.864	0.788	ACS Appl. Mater. Interfaces 2020, 12, 5, 5847-5856
NiFe-BDC (NH_2)	1.45	0.76	0.69	Angew. Chem. Int. Ed. 2020, 59, 5837-5843
Lattice strain NiFeMOF	1.53	0.83*	0.7*	Nat. Energy, 2019,4, 115-122
$NiCo_2S_4$@g-C_3N_4-CNT	1.56	0.76	0.8	Adv. Mater. 2019,31, 1808281
$CuMo_2ON$@NG	1.56	0.875	0.69	Nano Energy 2021, 85, 105987
CoFe@NC/KB-800	1.615	0.845	0.77	Chem. Eng. J. 2022, 427, 131614
CoFe@NC-SE	1.62	0.82	0.8	J. Power Sources 2020, 455, 227975
CoFe/N-GCT	1.67	0.79	0.88	Angew. Chem. Int. Ed. 2018, 57, 16166-16170
NiFe/N-CNT	1.52	0.75	0.77	Nano Eлergy 2020, 68 104293
Co-N-Cs	1.64	0.84	0.8	Adv. Funct. Mater. 2020, 30, 1908945
Ni-N_4/GHSs/Fe-N_4	1.62	0.83	0.79	Adv. Mater. 2020, 32, 2003134
Fe/N-G-SAC	1.6	0.89	0.71	Adv. Mater. 2020, 32, 2004900
(Fe,Co)-SA/CS	1.59	0.86	0.73	Small Methods 2021, 5, 2000751
CoNG900	1.61	0.86	0.75	Appl. Catal. B-Environ. 2021, 281, 119514
Pt/C||RuO_2	1.56	0.83	0.73	This work
CoFe@NOC	1.53	0.853	0.678	This work

Table S3. The performance of primary Zn-air batteries using various electrocatalysts.

Catalysts	Peak power density ($mW\ cm^{-2}$)	Durability (h)	Reference
Co/Co–N–C	132	~330	Adv. Mater. 2019, 31, 1901666.
$NiCo_2S4@gC_3N_4$-CNT	142	＞100	Adv. Mater. 2019, 31, 1808281.
MnO/Co/PGC	172	＞100	Adv. Mater. 2019, 31, 1902339.
Mn/Fe-HIB-MOF	195	1000	Energy Environ. Sci. 2019, 12, 727.
(Fe, Co)/CNT	260	~	Energy Environ. Sci. 2018, 11, 3375.
CoNi-SAs/NC	101.4	＞30	Adv. Mater. 2019, 0, 1905622.
N-$CoSe_2$/3D-MXene	142	166	ACS Materials Lett. 2019, 1, 432.
Co@N-PCP/NB-CNF-2-800	143.8	110	Appl. Catal. B-Environ. 2021, 286, 119888
1@ZIF-67	220	110	Angew. Chem. Int. Ed. 2021, 60, 8472-8476
Co_9-x$NixS_8$/NC	75	60	ACS Appl. Mater. Interfaces 2020, 12, 5847-5856
$(Co,Fe)_3N$	234		Nat. Commun. 2020, 11, 1952.
$CuMo_2ON$@NG	176.3	330	Nano Energy 2021, 85, 105987
CoFe@NC/KB-800	160	100 h	Chem. Eng. J. 2022, 427, 131614
CoFe@NC-SE	102	48 h	J. Power Souarces 2020, 455, 227975
Co-N-Cs	128	110 h	Adv. Funct. Mater. 2020, 30, 1908945
CoNi/BCF	155.1	30 h	Appl. Catal. B-Environ. 2019, 240, 193-200
Ni-N_4/GHSs/Fe-N_4	~	200 h	Adv. Mater. 2020, 32, 2003134
Fe/N-G-SAC	120	240 cycles	Adv. Mater. 2020, 32, 2004900
(Fe,Co)-SA/CS	83.65	100 h	Small Methods 2021, 5, 2000751
CoNG900	205.64	667 h	Appl. Catal. B-Environ. 2021, 281, 119514
H-Co@FeCo/N/C	125.2	200	Appl. Catal. B-Environ. 2020, 278, 119259
Pt/C||RuO_2	170	＞20	This work
CoFe@NOC	205	＞35	This work

Referance

[1] S. Mithun, J. Song, S. Jhung, *Chem. Eng. J.*, 2018, **331**, 124-131.

[2] L. Zhou, P. Zhou, Y. Zhang, B. Liu, P. Gao, S. Guo, *J. Energy Chem.*, 2021, **55**, 355-360.

[3] Y. Wang, L. Yan, D. Kamran, C. Zhao, X. Zhao, Y. Xue, J. Huo, S. Li, Q. Zhai, *Adv. Mater.* 2021, **33**, 2006351.

[4] X. Lu, Y. Chen, S. Wang, S. Gao, X. Lou, *Adv. Mater.* 2019, **31**, 1902339.